Modeling and experiments of a soft robotic gripper in amphibious environments

Yufei Hao, Tianmiao Wang, Ziyu Ren, Zheyuan Gong, Hui Wang, Xingbang Yang, Shaoya Guan and Li Wen

Abstract

This article presented the optimization parameter of a bidirectional soft actuator and evaluated the properties of the actuator. The systematic simulation was conducted to investigate the effect of the top wedged angle (the angle for the wedged shape of the actuator structure) of the chamber on the bending extent of the actuator when it is deflated. We also investigated the width of the actuator and the material combinations of the two layers with the relation to the deformation performance. A mathematical model was also built to reveal the deformation of the actuator as a function of the geometrical parameters of the inner chambers and the material properties. We quantitatively measured the bending radius and the actuation time of the actuator both in air and under water. Digital particle image velocimetry experiments were conducted under water to observe the flow patterns around the actuator. We found that the top wedged angle has a significant effect on the outward bending of the actuator when it is deflated, and 15° was found to be optimal for bending into a larger gripping space. The result shows that the actuator can deform much easier with a bigger width. Utilizing a soft gripper that was built by mounting four actuators to a three-dimensional-printed rigid support, we found that the prototype can grip objects of different sizes, shapes, and material stiffness in amphibious environments.

Keywords

Introduction

Soft robotics is a new interdisciplinary field involving chemistry,[1,2] biology,[3–5] material science,[6–8] and medical engineering,[9,10] and so on. Recently, the design, fabrication, and actuation of soft robotics have shown significant progress. The complex and compliant body of soft robots can be rapidly fabricated by taking advantage of shape deposition manufacturing,[11] soft lithography,[12,13] multi-material three-dimensional (3-D) printing,[14,15] and the combination of these technologies.[16] The representative actuation types of soft robots include fiber and tendon,[17] pneumatic artificial muscle,[18] fluidic elastomer actuator,[19] dielectric elastomer,[20,21] and shape memory alloy.[22] Soft actuators can achieve different locomotion by applying various actuation approaches. Soft pneu-net actuators can bend or rotate by pressurizing the channel networks confined by an inextensible layer.[23,24] Fiber-reinforced actuators can axially extend, radially expand, or twist just by varying the fiber angles.[25] By

Department of Mechanical Engineering and Automation, Beihang University, Haidian, Beijing, China

Corresponding author:
Li Wen, Department of Mechanical Engineering and Automation, Beihang University, 37 Xueyuan Rd, Haidian, Beijing 100191, China.
Email: liwen@buaa.edu.cn

integrating the two principles together, the actuators can elongate, twist, and bend in three-dimensional space.[26] To date, many researches have been done to exploit the potential applications of the soft robotics in the fields of biomimetic locomotion (such as swim and squirm[27–29]), manipulation,[30–32] medical and wearable devices,[10,33,34] and so on.

In our previous work, we developed a soft actuator that could perform basic gripping.[13] However, the optimal geometrical parameters of the chamber, which would significantly affect the deformation under pressurization or depressurization, have not yet been investigated. Some previous work has been carried out to investigate the geometry optimization of soft actuators such as the thickness of the outer layer of the chambers,[23,24] the height and number of the chambers,[24] the thickness of the actuators,[35] the shape of the chamber,[36] the fiber structures of the fiber-reinforced actuators,[37] and the effects of material properties,[38] and so on. Even the design and measurement of a bellow actuator for the linear motion were conducted.[39] However, three fundamental parameters, which have been proved to be critical for the soft actuator according to the tests in our lab, have not been studied yet: (1) the top wedged angle of the chambers, (2) the width of the actuator, (3) the material properties of the top layer and the lower layer. What if we change the structure of the chamber to a wedge shape? How does the width of the actuator influence the kinematics? Which kind of material combination should we use for different layers to improve the motion performance? To our knowledge, no previous study has investigated the questions above yet. Besides, very few studies have addressed under water grasping using soft robotics that could be a promising field for soft robotic systems in the future, for example, grasping live and delicate creatures under water without damage.

In this article, by improving the cross section of the chambers of the actuator in Mosadegh et al.,[24] we present a new structure for the soft actuator that can bend inward when inflated and outward when deflated. By using finite element analysis (FEA) simulation, we systematically investigated the relationship between the top wedged angles, the applied pressures, and the bending amplitude of the actuator while deflated. We also studied the effect of width and the combination of materials with different stiffness on the deformation. A mathematical model concerning the geometrical parameters of the chamber and the material properties was derived to describe the deformation principles qualitatively. To investigate the property of the actuator in amphibious environments, we quantitatively measured the actuation time and kinematics of the actuator both in air and under water. Digital particle image velocimetry (DPIV) experiment was conducted to visualize the flow patterns around the actuator. We then built a four-finger soft gripper which can be operated by a very simple gripping strategy: deflate the soft fingers to curl outward and open the gripper claw, then inflate the soft fingers to conform the objects when the gripper approaches them. The
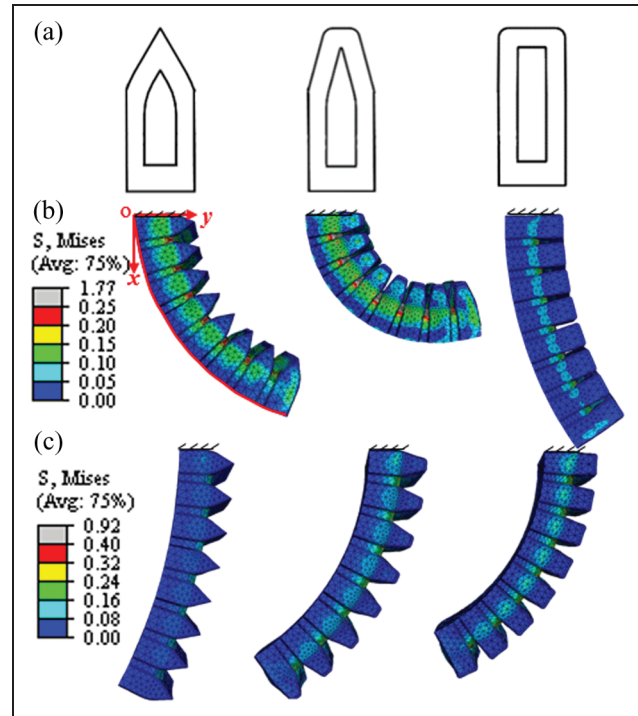

Figure 1. Typical finite element analysis (FEA) results under different θ of the actuator. (a) Schematic of the chamber shape. The angles θ are successively 30°, 15°, 0° from left to right. (b) The maximum bending angles of the three actuators when deflated. The applied pressures are −40 kPa for $\theta = 30°$ and 15°, and −10 kPa for $\theta = 0°$. The coordinate system and the profile curves of the lower layer used to calculate the bending radius are marked with solid red lines. (c) The FEA results of the three actuators at pressurization state. The applied pressure is 20 kPa.

gripping performance of the gripper was then evaluated by gripping multiple objects both in air and under water. The main contributions of the article are as follows: (1) investigate the effects of the top wedged angle, the width, and the combination of materials on the soft actuator bending kinematics; (2) investigate the kinematics and gripping performance of the soft actuator both in air and under water. The remainder of the article was organized as follows: in the second section, we introduced the simulation and the mathematical model for the soft actuator and then explained the experiments conducted in amphibious environments. In the third section, we demonstrated the results of the experiments. In the fourth section, we explained and discussed the reason for the results and drew some conclusions based on the analysis. In the fifth section, we provided a short conclusion on the whole article and the work as our next step.

Materials and methods

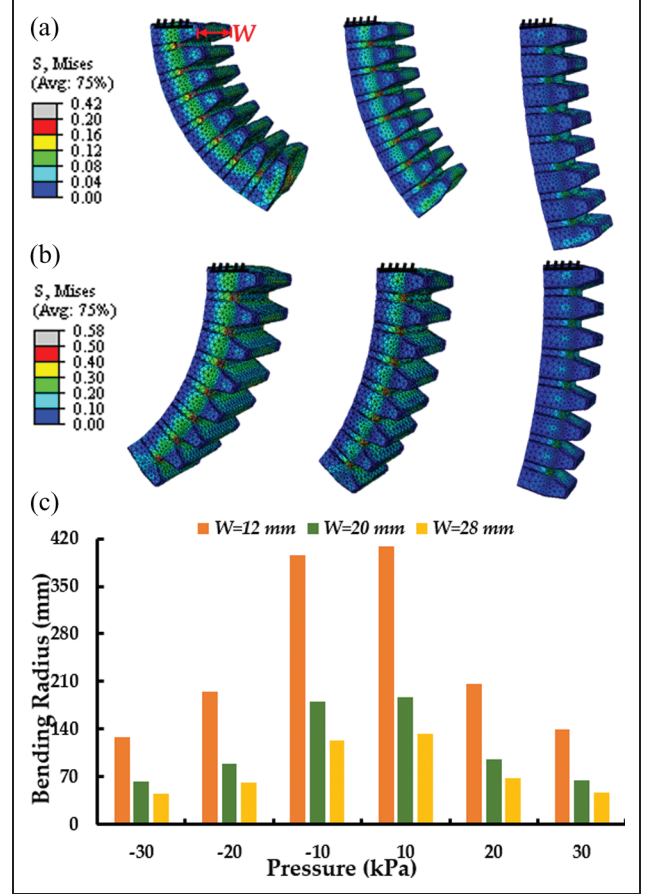### FEA simulation and mathematic model of the soft actuator

Compared with previous typical pneumatic networks that can bend in only one direction under pressurization,[24] our
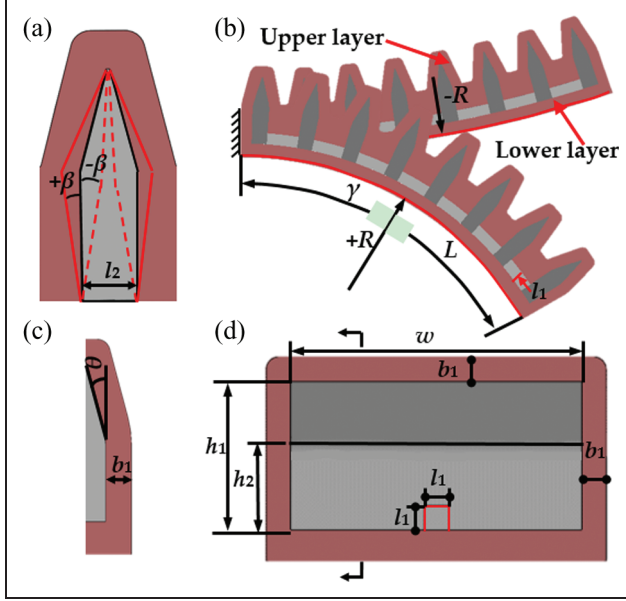
Figure 2. The illustration of the mathematic model and the geometric parameters of the soft actuator. (a) β indicates the bending angle generated by the pressurization or depressurization of the chamber. The positive sign "+" indicates the chamber under the pressurization state, while the negative sign "−" indicates the chamber under the depressurization state. $l_2 = 3$ mm. (b) The schematic of the bending radius R and total bending angle γ. A reverse bending is also shown in the model to demonstrate the depressurization state. The geometric parameters of one chamber are listed in (c) and (d). The parameters are $h_1 = 12$ mm, $h_2 = 7$ mm, $l_1 = b_1 = 2$ mm, $b_2 = 2.5$ mm, L 70 mm, respectively. The wedged angle is represented by θ and is also indicated in Figure 1(c).

Figure 3. The finite element analysis (FEA) results under different widths of the actuator (W). (a) The FEA results of the corresponding actuators under the depressurization state. The values for W are sequentially 28, 20, and 12 mm from left to right. The applied pressure is −20 kPa for the three actuators. (b) The FEA results of the three actuators under the pressurization state. The applied pressures are 20 kPa. (c) The bending radius of the soft actuators under different W as a function of applied pressure.

actuator can bend in both inward and outward directions, attributing the success to the wedged-like shape on top of the inner chamber. As Figure 1(b) shows, the soft actuator with a top wedged angle can bend outward when deflated. Besides, the width of the actuator and the combination of materials with different stiffnesses of the actuator's two layers (shown in Figure 2(b)) can also influence the deformation properties. In this article, we systematically studied the effect of the parameters above on the deformation characteristics of the soft actuator using the finite element analysis software Abaqus (Abaqus 6.12; SIMULIA Inc., France).

For the top wedged angle θ (shown in Figure 2(c)) simulation, we selected seven values from 0° to 30°, with an interval of 5° (if the angle is much bigger, the height of the actuator will diminish). In the simulation, the material properties were set the same as dragon skin 30 (Smooth-On Inc., Macungie, Pennsylvania, USA). An incompressible hyperelastic Mooney–Rivlin model with an elastic modulus (E) of 1 Mpa[17] and Poisson ratio (μ) of 0.49 was used to build the nonlinear properties of the material. The self-contact interaction property was set on all the outer surfaces and the inner walls of the actuator to simulate the

interacting conditions of the surfaces under big pressures. A pinned constraint was enforced on one end of the actuator to restrict the displacements in the x, y, and z directions. The pressure was exerted on all the inner walls of the chambers. A 10-node quadratic tetrahedron hybrid element type (C3D10 H for Abaqus) was used to mesh the two layers of the actuators. The models were analyzed using ABAQUS/Standard for the quasi-static nonlinear simulation. After simulation, the coordination values of the profile curve of the lower layers (showed in Figure 1(b)) were obtained and the bending radius of the profile curve was calculated by a self-developed Matlab program (Matlab 2014; MathWorks Inc., Natick, Massachusetts, USA) using the least square method.

For the simulation on width (W) (showed in Figure 3), the width values were set to 12, 20, and 28 mm, which are within our design parameter limits (10–30 mm) in consideration of the air consumption, with fixed θ at 15°. The simulation procedures were similar to the wedged angle

simulation process. For the simulation on different material combinations, the angle θ was set to 15° and the width W was 28 mm. Three models were established for simulation. For the first model, the materials for the upper and lower layers were dragon skin 10 (Smooth-On Inc.) and dragon skin 30, respectively. For the second model, both the layers were dragon skin 30. For the last model, the materials for the upper and lower layers were dragon skin 30 and dragon skin 10, respectively. According to the literature,[40] the property of dragon skin 10 was built as a Yeoh model, and the material coefficients were $C1 = 0.036$ MPa, $C2 = 2.58E-4$ MPa, and $C3 = -5.6E-7$ MPa. Based on simulation results, we fabricated the soft actuators with the parameter θ to 15°, W to 28 mm as the optimum value for our current application and used dragon skin 30, which we used mostly, for both the layers of the soft actuator to conduct the physical experiments.

Inspired by the mathematical modeling method in Onal et al.,[41] a mathematic model that captures both the geometrical properties of the chamber and the applied pressures was established to describe the deformation (shown in Figure 2). In order to simplify the model and neglect some minor factors, we made a few simplifications: (1) the length L of the lower layer of the actuator is assumed to be constant; (2) the actuator has no radial expansion; (3) the effect of the channel that connects each chamber unit is negligible as its size is significantly smaller than the width w and height h_1 of chamber (as shown in Figure 2(d)); (4) the chambers deform mainly through extending the side walls, and the deformation of the surfaces of the chambers is neglected. Because all the chambers have the same geometrical structure, we calculated the bending angle of one chamber then integrated them together. For a single chamber unit, the axial (the deformation direction of the actuator) stress σ_x is as follows:

$$\sigma_x = \frac{Pwh_2 + Pcos\theta w(h_1 - h_2)}{2h_1 b_1 + (w + 2b_1)b_1} \quad (1)$$

where P is the pressure applied on the inner wall of the chamber, w is the width of the chamber, h_1 is the total height of the chamber, and h_2 is the height of the bottom rectangle. The deformation of the chamber along the axial direction is

$$D_x = l_2 \varepsilon_x(\sigma_x) \quad (2)$$

where l_2 is the initial distance between the two walls of the chamber and ε_x is the strain, a function of the stress σ_x, which can be obtained by calibration. For the specific actuator parameters we selected after the simulation ($\theta = 15°$, $W = 28$ mm, and dragon skin 30 as the material), we obtained the function to calculate the bending radius and compared the results with the physical experiment in the following section to verify the model. To get the function, we obtained the distance between the walls of the chamber under different pressures in the simulation, then fit the data in Matlab by a self-developed program. A quadratic
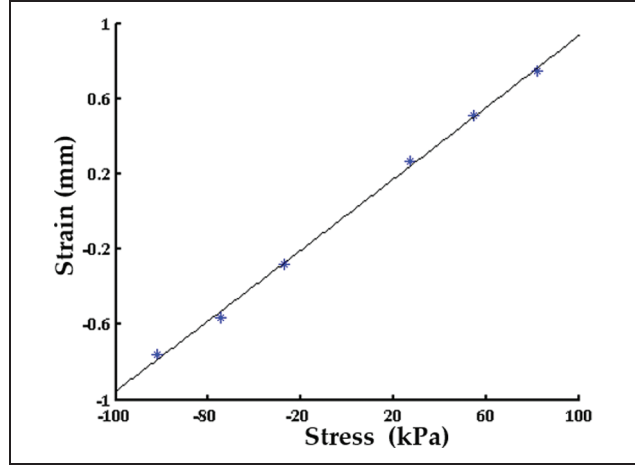
Figure 4. The fitting function of the strain–stress relation for the soft actuator.

polynomial fitting function was obtained to describe the relationship between ε_x and σ_x (Figure 4 shows the fitness of the function for the data):

$$\varepsilon_x(\sigma_x) = 6.35^*10^{-7}\sigma_x^2 + 9.4^*10^{-3}\sigma_x - 0.017 \quad (3)$$

Because the inextensible bottom layer constrains the elongation/contraction of the top layer, the soft actuator generates a bending deformation. The bending angle β of the chamber wall (as Figure 2(a) shows) is

$$\beta = \tan^{-1}\frac{l_2\varepsilon_x(\sigma_x)}{2h_2} \quad (4)$$

The total bending angle γ of the actuator can be calculated by integrating all the bending angles of the chambers

$$\gamma = 2n\beta \quad (5)$$

where n is the number of chambers, and in the present study $n = 8$. The bending radius of the actuator R is

$$R = \frac{L}{\gamma} \quad (6)$$

To make the mathematic model also suitable for the depressurization state, we assume that the bending angle β is negative when a negative pressure is applied to the chamber walls. Therefore, the corresponding bending radius R is also negative (as Figure 2(b) shows).

Experiments of the soft actuator and soft gripper

The soft actuator was made in purely soft materials and actuated by pneumatics, so it has inherent advantages for the amphibious applications. Based on the simulation results, we fabricated a soft actuator with $\theta = 15°$, $W = 28$ mm, and dragon skin 30 as the material for the physical experiments and the validation of the simulation. A tip structure (as Figure 5(a) shows) was designed for the
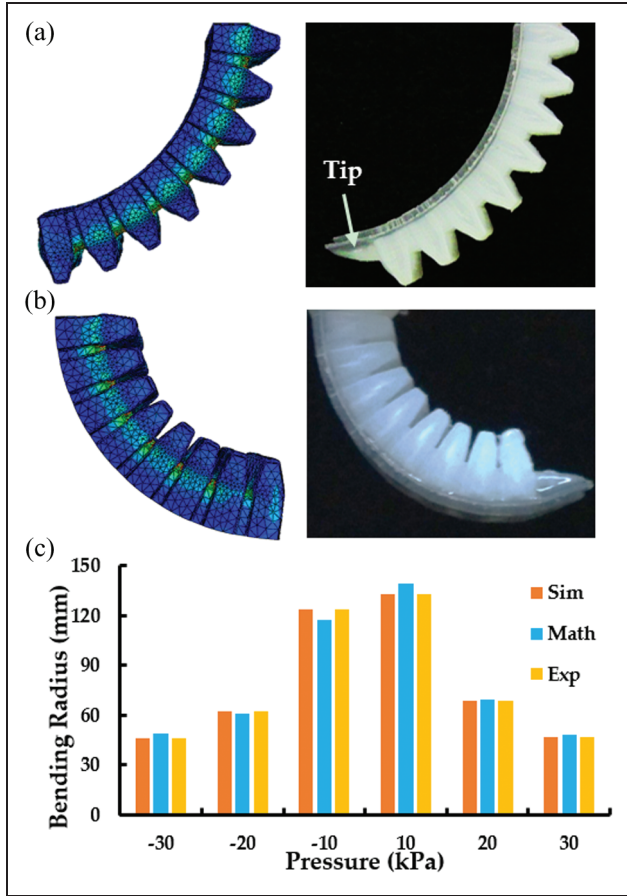
Figure 5. The comparisons of results between FEA simulation, mathematic model, and experiment conditions. (a) The comparison between simulation and experiment at the pressurization state. The pressure applied is 20 kPa. (b) The comparison between simulation and experiment at the depressurization state. The pressure applied is −30 kPa. (c) The bending radius as a function of pressure for the simulation, mathematic model, and experiment results. The "Sim," "Math," and "Exp" correspondingly mean the simulation, mathematic model, and experiment. The absolute radius values were used for the mathematical model.

purpose of pinch operation. The fabrication process was similar to our previous article,[13] which is "soft lithography" and commonly used for the fabrication of soft robotics.[1,12] Two experiments were conducted to evaluate the performance of the actuator both in atmosphere and under water. The first experiment was to compare the kinematics and actuation time in amphibious environments. The actuation time is defined as the time needed for the actuator to reach a steady state under a certain pressure. A shadow water tank was used to build an underwater environment, and the actuator was set at about 0.2 m deep under the water surface. For the comparison of kinematics, we inflated the soft actuator to a certain pressure (from −30 kPa to 30 kPa with an interval of 10 kPa) and obtained the kinematic data both in air and under water. The coordinate values of the profile curves of the lower layer during motion were digitized using a self-developed Matlab program, and the bending
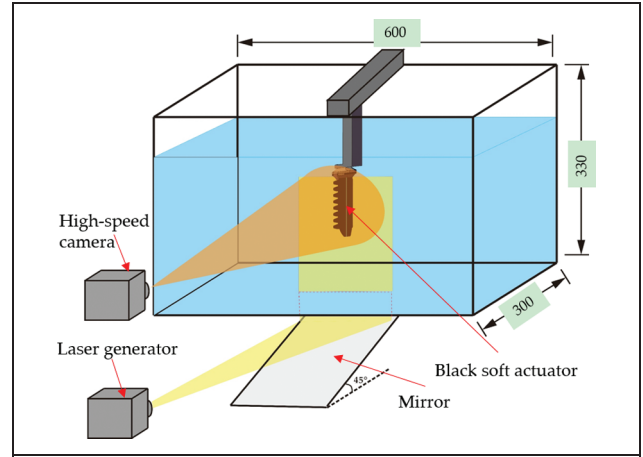

Figure 6. The DPIV experiment setup.

radius of the actuator was calculated by least square method. For the comparison of actuation time, we inflated the actuator to a preset pressure immediately and captured the deformation process of the actuator simultaneously via a camera. Then the actuation time was derived by a vision process program. The pressures we selected in this test were from 5 kPa to 30 kPa with an interval of 5 kPa.

To investigate the kinematics of the soft actuator in underwater environments, DPIV experiments were conducted to obtain the flow patterns around the actuator while it performs actions. As Figure 6 shows, the tests were conducted in a glass water tank measuring 600 × 300 × 330 mm. The soft actuator was arranged vertically, fully submerged in the water. To avoid the wall effect, the distance between the tip of the actuator and the tank bottom was kept larger than 100 mm. To diminish the influence of the light reflection, the actuator body was coated with a thin layer of black silicone rubber. The water was seeded using near neutrally buoyant glass beads with a diameter of 20 μm. A laser sheet with a thickness of 1.5 mm was projected vertically from the bottom of the water tank to illuminate the particles around the actuator. A high-speed camera (FASTCAM Mini UX100; Photron Inc., Japan) was applied to track the movement of the particles with an acquisition rate of 500 HZ. The image sequence was subsequently input into a commercial DPIV calculation software (MicroVec; LiFangTianDi Inc., China) to obtain the velocity field of a certain time instant. Two experiments were carried out: (1) single actuator movement including pressurization and depressurization processes and (2) pinch operation of a two-finger gripper by integrating two actuators to a support.

A four-finger soft robotic gripper was built by connecting four soft actuators to a support using some hard components. The air inlets of the four actuators were connected to a One-Touch Fitting (KQ2UD04; SMC Inc., Japan) so that the four actuators could be actuated simultaneously. The inlet of the One-Touch Fitting was connected to an
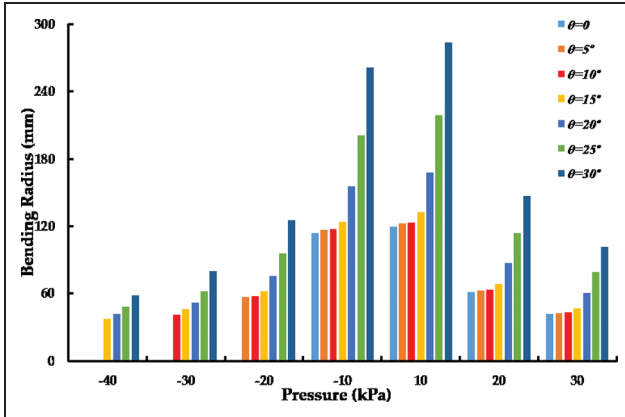
Figure 7. The bending radius of the soft actuators under different θ as a function of applied pressure. The coordinate system and the corresponding profile curves are demonstrated in Figure 1.

electropneumatic proportional pressure valve (ITV0030; SMC Inc.) which was used to control the air pressure by changing analog voltage input. An innovative grasping approach was proposed based on the bidirectional motion of the soft actuator with two steps: (1) deflate the soft actuator to curl outward so that the gripper can approach the object and (2) inflate the actuator to curl inward so that the gripper can contact with the surface of the object and exert a lift force on the object when moving upward. To evaluate the grasping performance of the gripper, we used the gripper to grip some common objects with different sizes, shapes, and material stiffness both in air and under water.
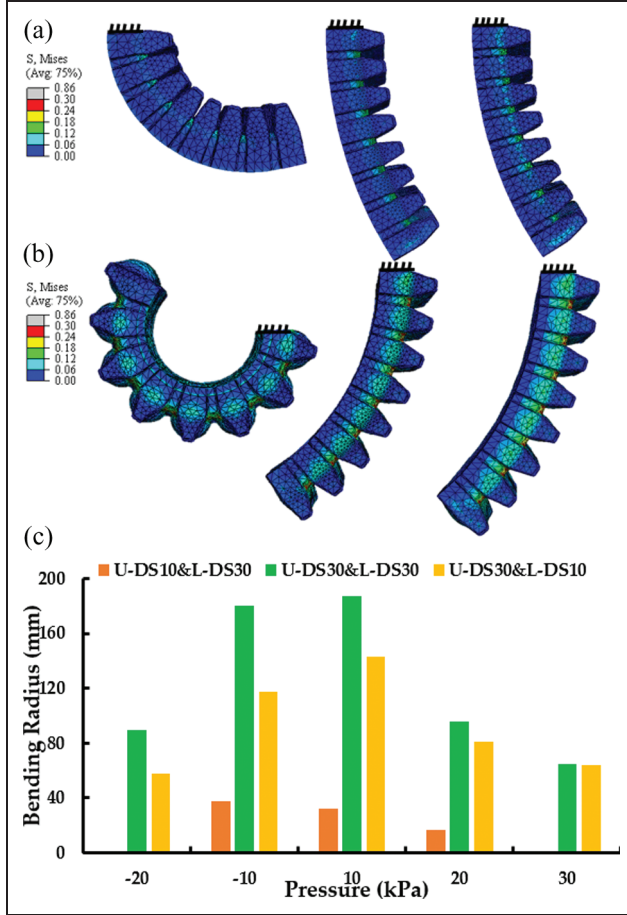
Results

Geometric effect of the chamber

The FEA simulation results of the effect of θ are shown in Figures 1 and 7. Figure 1 shows the motion analysis of three typical models under both depressurization and pressurization states. The θ values for these models are 30°, 15°, and 0° (shown in Figure 1(a) from left to right). Figure 1(b) shows the kinematics of the actuators when the three θ values were under the depressurization state. It is obvious that the actuator has the maximum bending angle when θ is 15° and the minimum bending angle when θ is 0°. It should be noted that the applied pressure for $\theta = 0°$ is -10 kPa while the pressure for the other two models is -40 kPa, because the actuator has reached the maximum deformation extent under -10 kPa for $\theta = 0°$ in the simulation. The motion analyses for the pressurization state are depicted in Figure 1(c). The applied pressures are 10 kPa for the three models. It can be observed that the actuators have similar bending angles when $\theta = 0°$ and $\theta = 15°$, which is smaller than that when $\theta = 30°$. Figure 7 describes the bending radius of the soft actuator under different θ as a function of the applied pressure. For $\theta = 0°$, the values from -40 kPa to -20 kPa are missed. For $\theta = 5°$, the values at -40 kPa
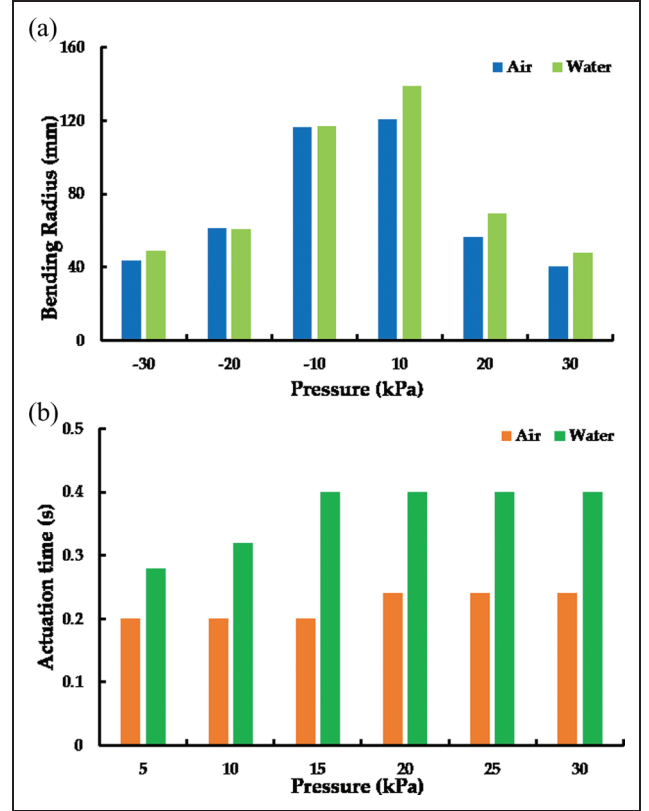
and -30 kPa are missed. And for $\theta = 10°$, the value at -40 kPa is missed. The missed values mean that the simulation results are nonconvergence at the corresponding pressures, indicating the actuators had achieved the deformation limitation before the pressures were applied. With the absolute value of pressure increasing, the bending radius for all the θ values decreases, which means the actuator undergoes greater deformation for a bigger pressure. For θ from 0° to 15°, the bending radius has a little increment under the same pressures. When θ surpasses 15° to reach 30°, the bending radius increases significantly for the same pressure. This phenomenon demonstrates that the angle θ indeed has an influence on the deformation of the actuator, which decides the maximum bending limitation for the depressurization state and influences the deformation behaviors for the pressurization state. Synthesizing all the results, we conclude that the 15° is the best value for θ, for which the actuator can achieve the maximum bending extent when deflating. Besides, the bending radius of the actuator with $\theta = 15°$ may be a little bigger compared to those ranging from 0° to 10°, but much smaller compared to the actuators ranging from 20° to 30°.

The FEA results about the width parameter of the actuator (W) are demonstrated in Figure 3. Figure 3(a) shows the depressurization state of the actuators under pressure -20 kPa, it is evident that the wider the actuator, the bigger bending deformation it can achieve, which has a similar tendency to the experiment results on pressurization (shown in Figure 3(b)). Figure 3(c) presents the bending radius of the actuator under different W as a function of applied pressure. It is obvious that the actuator has smaller bending radii when applied bigger pressures. For all the pressure values, it can be testified that the actuator will reach a smaller bending radius with the W increasing. Based on the experiment results, we can conclude that the actuator will deform easier under both the depressurization and pressurization states if it has a larger width. Figure 8 describes the FEA results under different combinations of materials in the two layers of the actuator. Figure 8(a) and (b) shows the motion analysis of the actuators with different material combinations under the depressurization and pressurization states separately. In Figure 8(c), the values are missed at the pressure -20 and -30 kPa for the actuator which uses dragon skin 10 for the upper layer and dragon skin 30 for the lower layer, because the actuator has reached the deformation limitation before these pressures. From -10 kPa to 20 kPa, it can be verified that the actuator will have a smaller bending radius by changing the material to softer ones for the upper layer under the same pressures. By comparing the bending radius of actuators with different materials for the lower layer but the same material for the upper layer, it can be obtained that the actuator will have a smaller bending radius with a soft material for the lower layer. But the gap diminishes when the absolute value of pressure increases.

Figure 8. The finite element analysis (FEA) results under different material combinations of the actuator. For the left model, we used dragon skin 10 for the upper layer and dragon skin 30 for the lower layer, represented as "U-DS10&L-DS30." For the middle model, the materials of the two layers were both dragon skin 30 represented as "U-DS30&L-DS30." For the right model, the materials for the upper and lower layers were dragon skin 30 and 10, respectively, represented as "U-DS30&L-DS10." (a) The FEA results under the depressurization state. The pressures are −10 kPa for the three actuators. (b) The FEA results under the pressurization state. The applied pressures are 20 kPa. (c) The bending radius of the soft actuators under different material stiffness combinations as a function of applied pressure.


Figure 9. The bending radius and actuation time comparisons under water and air environments. (a) The bending radius as a function of pressure in air and water environments. (b)The actuation time as a function of pressure in air and water environments.

To verify the results of simulation and mathematical model, we compared the kinematic data from the simulation and the mathematical model with that of the physical experiments under water. Figure 5 shows the corresponding results. From the images shown in Figure 5(a) and (b), we can see that the simulation results agree well with the physical experiment under both depressurization and pressurization states. It can be verified that the small tip of the actuator prototype has little influence on the kinematics but improves the grasping performance (this can be proved by the grasping experiments of the soft gripper). From Figure 5(c), it can be observed

that the mathematical and simulation results agree well with the physical experiment results for most of the pressure values. For the pressure −10 kPa and 10 kPa, the error is relatively bigger. It should be noted that both the mathematical model and the simulation neglected the influence of gravity, for the gravity is relatively slight. Besides, the physical experiment was conducted under water to diminish the influence of gravity.

Gripping performance of soft actuator in air and water

The results of comparison between kinematics and actuation time in amphibious environments are demonstrated in Figure 9. It can be observed from Figure 9(a) that there is a little difference between the bending radii under depressurization state in air and under water. For the pressurization state, the bending radius in water is a little bigger than that in air. But the difference is reduced with the increase in pressure. Though there exists some difference, the bending radius obtained under water only surpasses that in the atmosphere by 13.3% at most (when the pressure is 10 kPa). Therefore, we speculate that the actuator may have similar kinematics in the air and shallow water. From Figure 9(b), it is evident that the actuation time is
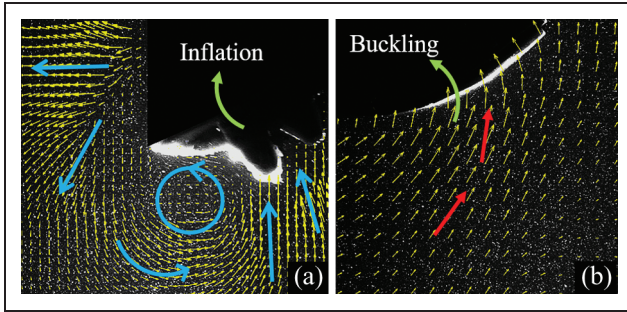
Figure 10. The flow pattern around the finger during (a) pressurization and (b) depressurization process under water.

much longer in water than that in air. The reason may be that the actuator undergoes more resistance in water, for the density of water is much larger than that of air. For the same medium, the actuation time is similar when the pressure increases (the error of the video frame rate is 0.04 s). So we speculate that the applied pressure may not influence the actuation time and the actuator has a fast response speed (less than 0.4 s).

The bending movement of a single actuator when pressurized caused a distinct vortex clinging to the dorsal side of the tip, as indicated in Figure 10(a) with a blue vector circle. The flow near the tip seems to rotate about the vortex core strongly. When the actuator was exhausted, it would buckle outward and hence "suck" the flow upward, as shown in Figure 10(b). The flow direction seems to follow the trace of the bending actuator. When two-finger gripper conducted pinch operation under water, similar tip vortexes can be observed. However, the position of the vortex shifted to the ventral side of the tip, migrating forward compared to the vortex found in single actuator bending (as shown in Figure 11(a)). Since two actuators were actuated with a pump simultaneously, the bending movement of one actuator was an exact mirror movement of another one. Hence the vortexes induced were equal in magnitude while opposite in direction. The flows between two actuators should also be noted. The green dashed line in Figure 11 indicated a boundary of flows with different directions. Above the dashed line, the flows were pushed obliquely upward, while below the boundary, the flows were directed obliquely downward and finally formed a strong downward jet. If two actuators further approached, these two tip vortexes would be shed downward and finally shifted to the dorsal side of the tip when two tips finally collided (as shown in Figure11(b)).

With the inherent compliance property, the soft gripper can efficiently conform and grip objects without complicated control systems. Experiments indicate that the gripper performs well both in air and under water. As Figure 12 shows, the gripper can successfully grasp a sphere with a diameter of 170 mm, about 2.43 times the length of the actuator. It can grip an approximate 250 g cup in the lateral direction without vibration, pinch a 3 mm screw using two fingers. For the under water experiments, the gripper can enclose a bundle of scaphium scaphigerum and take it out of the water without

damage. It can grasp a smooth soap and a small grape. A video (supplementary material) recording the gripping process demonstrates the capability of the universal soft gripper.

Discussion

FEA simulation

Systematic studies in this article have demonstrated that the top wedged angle contributes to the outward bending of the soft actuator. As Figure 7 shows, a smaller anti-bending radius can be obtained under a bigger negative pressure. However, according to our simulation, only when θ is set bigger than $15°$, it can reach such an extent (when the pressure arrived -40 kPa) because the gaps between the neighboring two chambers increase with the increment of θ, diminishing the resistance and increasing the space for deflation. When the pressure is fixed, the bending radius increases monotonously with the growth of θ. This phenomenon could be explained by the mathematical model. According to equation (1), as θ increases, the stress σ_x decreases. So the strain and the bending angle will decrease and the bending radius increases. Furthermore, the radius increases dramatically from $15°$ to $30°$, because the bigger θ will cut down the height of the chamber when other geometry parameters keep constant. The width of the actuator has a significant influence on the kinematics of the actuator, which can be verified by Figure 3. According to the results, we hypothesize that the kinematical performance of the actuator for both depressurization and pressurization states will be significantly improved by increasing the width. For the actuator with a bigger width could generate more force to conquer the internal stress of the material under the same pressures. Nevertheless, a bigger width requires more air volume and therefore results in a slower actuation speed. Based on the results of Figure 8, we speculate that materials of the upper layer of the actuator have a major effect on the motion performance. The softer the material for the upper layer, the easier the actuator deforms. Although the actuator with a softer material for the lower layer also has a smaller bending radius, this difference is not as distinct as that of the actuator with a softer upper layer. We speculate this difference may be caused by the special topographical structure of the top layer, which contributes to the bending motion of the actuator.

Based on the simulation results, we summarized some empirical criteria that can help us optimize the actuator structure for a specific application. (1) If we want the soft gripper to grasp much bigger objects, it is better that the soft actuator has a top wedged shape which could make the actuator to bend outward and open the working space. And the angle of the top wedge should be approximately $15°$, which has the biggest reverse bending extent. (2) By increasing the width, the actuator can bend more easily, and more force can be exerted under the same pressure. However, the wider the actuator, the more air will be
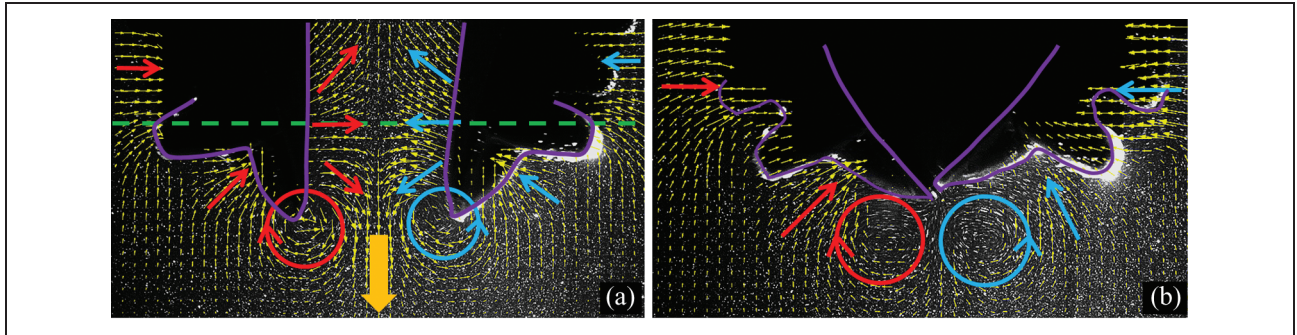
Figure 11. The flow pattern around during pinch operation under water. (a) Two actuators were approaching. (b) The tips contacted.
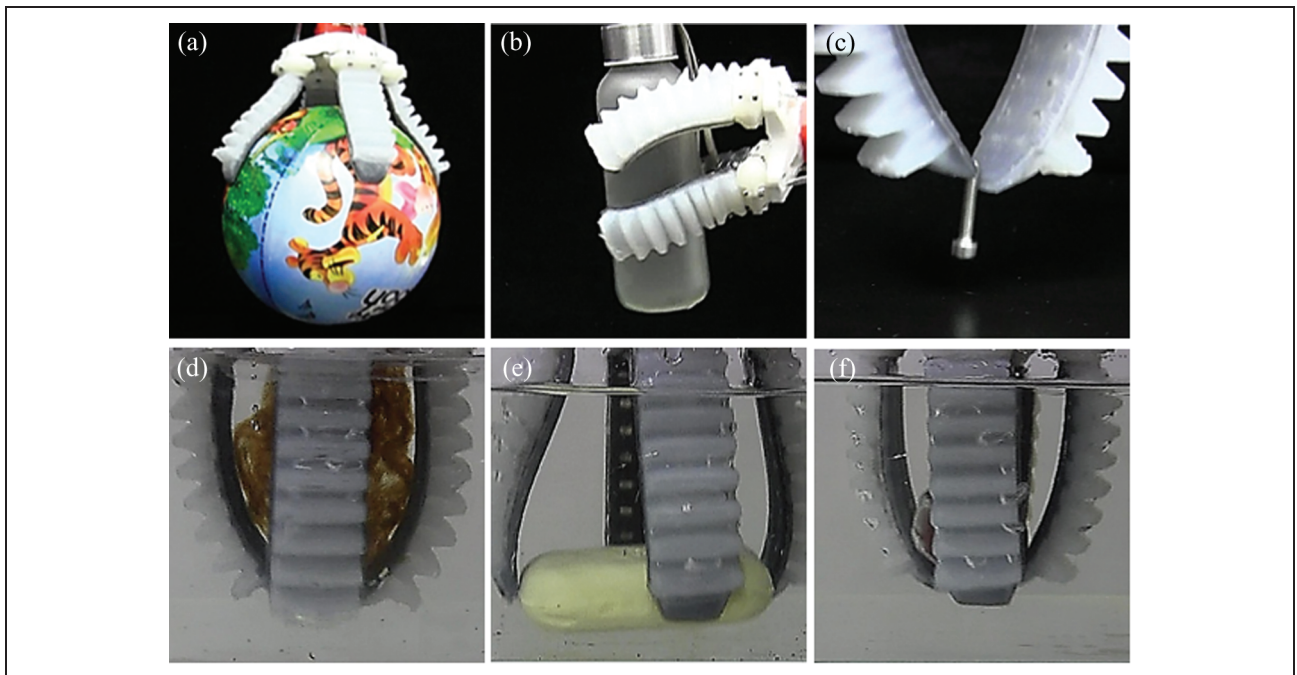
Figure 12. Results about the gripping performance of the soft gripper in amphibious environments. The gripper can successfully grasp (a) a sphere with a diameter of 170 mm, (b) a cup with a weight about 250 g, (c) a screw with a diameter of 3 mm, (d) a bundle of scaphium scaphigerum, (e) a piece of soap, and (f) a grape.

needed for the actuator since it has a bigger volume, and the response speed will slow down too. So, within the limit of the air consumption for the control system and the response time, it is better that the actuator has a bigger width. (3) With a softer upper layer, the actuator can bend more easily. However, the exerted force may decrease.

The simulation was conducted by varying only one parameter, keeping the others constant. It will be more significant if we could simulate the parameters together to find the best design. However, it is a challenging work because it needs much knowledge such as material physics, mechanics of materials, theoretical mechanics, FEA, and some design experience and optimization criteria. If we could deal with these problems step-by-step, developing a software to optimize the soft actuator will come true. Besides to quantitatively compare the influence of the geometrical parameters on the kinematics of the actuator, we

set the shape of the actuator as rectangle. It should be noted that actuators with other shapes can also achieve the bidirectional motion if they have a top wedged angle to increase the space for deflation, the same actuation principle as the rectangular one. But different shapes were described by different geometrical parameters. It is very difficult to quantitatively compare the influence of the shape difference on the kinematics of the actuator, and new quantitative metrics should be made.

Mathematical model

The mathematical model has similar drawbacks listed in Marchese et al.,[4] such as the neglect of the forces generated by the antagonistic half of the chamber units and the inapplicability for big deformation. But it can qualitatively analyze the effect of geometry parameters such as the top

wedged angle, width of the actuator, height and thickness of the chamber on the actuator's deformation performance. The accuracy of the mathematical model was guaranteed by fitting the function about the strain–stress relationship of the material. This function described the nonlinear property of the material and could be used for the curve control but did not give a clear explanation of the material model, which is a difficult problem for large deformation theory. Errors exist between the results of simulation and physical kinematical experiments. Three major reasons may cause this: (1) mechanical error exists for the fabrication of the mould, (2) when doing the physical experiment, the pressure values were tested by the pressure sensor that has error tolerance (± 0.2 kPa), and (3) there also exist some errors in the simulation, such as the element types and mesh density.

Experiments in amphibious environments

There is no significant difference between deformation amplitudes in the two circumstances (see Figure 9(a) for indication). Since the deformation amplitude hinges on the differential pressures between the inner chamber and the external environment, which were kept the same in air and under water environments. However, the differences in actuation speed do exist, the actuator moving significantly slower in water than in air (as Figure 9(b) shows). It is the direct consequence of the water resistance, which is much higher than that in the air. An additional explanation is that since the external pressure under water is higher than that in the atmosphere, we need to inflate more air into the inner chamber to reach a certain pressure, which prolongs the actuation time. It is quite interesting that the actuation time didn't change significantly under different air pressures in the same medium. Hence, we speculate that the actuator is not sensitive to the pressure variation. And the driving system (including the pressure of the compressor, the frequency of the electric proportional valves, and the diameter of the tubes, and so on) may be the dominant factor for the actuation speed. DPIV experiments show that the actuator can generate observable vortex when interacting with water. Besides the morphology of the vortex when two or more actuators moved simultaneously was different from that generated by a single actuator. The upward flows between two counter vortexes are supposed to be helpful for grasping (as shown in Figure 11(a)). We hypothesize that the upward flow can be enhanced and the downward flow can be diminished by changing the actuator's morphology or switching the grasping strategy.

Maybe the soft gripper cannot lift heavy objects compared to traditional grippers and jamming gripper,[42] but it has an overwhelming superiority in gripping soft and fragile objects. As Figure 12(d) and (f) shows, it can grasp a cluster of scaphium scaphigerum and grape. This kind of work is impossible for a hard gripper, even for the jamming gripper. Based on the gripping performance experiments,

we summarize four gripping modalities: opposed pinch, spherical pinch, spherical power, and lateral power. For the tiny objects, such as the screw showed in Figure 12(c), the gripper can gently pinch them with two fingers (opposed pinch). For the small and short objects (as Figure 12(e) and (f) shows), the gripper can pinch them spherically. For the big size objects, the gripper uses the spherical power strategy shown in Figure 12(a). For the long objects (like the cup showed in Figure 12(b)), the gripper can grasp them from the lateral direction (lateral power).

Conclusion

In this article, we described the process for morphology parameter optimization of a soft actuator utilizing FEA simulation. The top wedged angle, the width, and the combination of different materials were firstly incorporated. A mathematical model was then developed to explain how these parameters work on the kinematic performance. Optimal parameters were then selected to achieve maximum bending amplitude under both pressurization and depressurization states and applied to build an actuator prototype. Systematic physical experiments were then conducted on the actuator in amphibious environments. Significant characteristic on operation performance was observed both in air and under water, including the bending radius and the actuation time. DPIV experiments clearly revealed the vortexes between two interacting soft actuators, which may be helpful for under water grasping. A four-finger gripper prototype based on the soft actuator was developed and showed excellent grasping ability in amphibious environments, especially for soft and fragile objects. However, the structure of the actuator may not be the optimum one for under water grasping, for the gripper may undergo unexpected vortexes and flow resistance when operating in running water. In the future, we may develop a suction gripper that uses suction flows to enhance the grasping for small, lightweight floating objects or suspended objects in the water, and we optimize the parameters of the soft actuator as a group to find the global optimum and optimize the bidirectional motion of the acutator by attempting different chamber shapes.

Declaration of conflicting interests

Funding

Supplemental Material

The online [appendices/data supplements/etc] are available at http://journals.sagepub.com/doi/suppl/10.1177/1729881417707148.

References

1. Morin SA, Shepherd RF, Kwok SW, et al. Camouflage and display for soft machines. *Science* 2012; 337(6096): 828–832.

2. Ilievski F, Mazzeo AD, Shepherd RF, et al. Soft robotics for chemists. *Angew Chem Int Ed* 2011; 50(8): 1890–1895.

3. Raphael D and Brock O. A novel type of compliant and under-actuated robotic hand for dexterous grasping. *Int J Robot Res* 2016; 35(1–3): 161–185.

4. Marchese AD, Onal CD, and Rus D. Autonomous soft robotic fish capable of escape maneuvers using fluidic elastomer actuators. *Soft Robot* 2014; 1(1): 75–87.

5. Cianchetti M, Calisti M, Margheri L, et al. Bioinspired loco-motion and grasping in water: the soft eight-arm OCTOPUS robot. *Bioinspir Biomim* 2015; 10(3): 035003.

6. Roche ET, Wohlfarth R, Overvelde JT, et al. A bioinspired soft actuated material. *Adv Mater* 2014; 26(8): 1200–1206.

7. Mac Murray BC, An X, Robinson SS, et al. Poroelastic foams for simple fabrication of complex soft robots. *Adv Mater* 2015; 27(41): 6334–6340.

8. Shen Q, Wang T, Liang J, et al. Hydrodynamic performance of a biomimetic robotic swimmer actuated by02ionic polymer–metal composite. *Smart Mater Struct* 2013; 22(7): 2896–2912.

9. Park YL, Chen B, Pérez-Arancibia NO, et al. Design and control of a bio-inspired soft wearable robotic device for ankle-foot rehabilitation. *Bioinspir Biomim* 2014; 9(1): 016007.

10. Ranzani T, Gerboni G, Cianchetti M, et al. A bioinspired soft manipulator for minimally invasive surgery. *Bioinspir Biomim* 2015; 10(3): 035008.

11. Gafford J, Ding Y, Harris A, et al. Shape deposition manu-facturing of a soft, atraumatic, and deployable surgical gras-per. *J Mech Robot* 2015; 7(2): 021006.

12. Shepherda RF, Ilievskia F, Choia W, et al. Multigait soft robot. *Proc Natl Acad Sci USA* 2011; 108(51): 20400–20403.

13. Hao Y, Gong Z, Xie Z, et al. Universal soft pneumatic robotic gripper with variable effective length. In: *Control conference (CCC), 2016 35th Chinese. TCCT*, Chengdu, China, 27–29 July 2016, pp. 6109–6114. IEEE.

14. MacCurdy R, Katzschmann R, Kim Y, et al. Printable Hydraulics: a method for fabricating robots by 3D co-printing solids and liquids. In: *2016 IEEE international conference on robotics and automation (ICRA)*, Stockholm, Sweden, 16–21 May 2016.

15. Bartlett NW, Tolley MT, Overvelde JTB, et al. A 3D-printed, functionally graded soft robot powered by combustion. *Science* 2015; 349(6244): 161–165.

16. Cho KJ, Koh JS, Kim S, et al. Review of manufacturing processes for soft biomimetic robots. *Int J Precis Eng Manuf* 2009; 10(3): 171–181.

17. Manti M, Hassan T, Passetti G, et al. A bioinspired soft robotic gripper for adaptable and effective grasping. *Soft Robot* 2015; 2(3): 107–116.

18. Kang R, Branson DT, Zheng T, et al. Design, modeling and control of a pneumatically actuated manipulator inspired by biological continuum structures. *Bioinspir Biomim* 2013; 8(3): 036008.

19. Tolley MT, Shepherd RF, Mosadegh B, et al. A resilient, untethered soft robot. *Soft Robot* 2014; 1(3): 213–223.

20. Shian S, Bertoldi K, and Clarke DR. Dielectric elastomer based "grippers" for soft robotics. *Adv Mater* 2015; 27(43): 6814–6819.

21. Shintake J, Rosset S, Schubert B, et al. Versatile soft grippers with intrinsic electroadhesion based on multifunctional poly-mer actuators. *Adv Mater* 2016; 28(2): 231–238.

22. Seok S, Onal CD, Cho KJ, et al. Meshworm: a peristaltic soft robot with antagonistic nickel titanium coil actuators. *IEEE/ASME Trans Mech* 2013; 18(5): 1485–1497.

23. Sun Y, Song YS, and Paik J. Characterization of silicone rubber based soft pneumatic actuators. In: *IEEE/RSJ international conference on intelligent robots and systems (IROS)*, Tokyo, Japan, 3–7 November 2013.

24. Mosadegh B, Polygerinos P, Keplinger C, et al. Pneumatic networks for soft robotics that actuate rapidly. *Adv Funct Mater* 2014; 24(15): 2163–2170.

25. Connolly F, Polygerinos P, Walsh CJ, et al. Mechanical pro-gramming of soft actuators by varying fiber angle. *Soft Robot* 2015; 2(1): 26–32.

26. Suzumori K, Iikura S, and Tanaka H. Applying a flexible microactuator to robotic mechanisms. *IEEE Control Syst* 1992; 12(1): 21–27.

27. Suzumori K, Endo S, Kanda T, et al. A bending pneumatic rubber actuator realizing soft-bodied manta swimming robot. In: *2007 IEEE international conference on robotics and auto-mation*, Roma, Italy, 10–14 April 2007, pp. 4975–4980. IEEE.

28. Sfakiotakis M, Kazakidi A, and Tsakiris DP. Octopus-inspired multi-arm robotic swimming. *Bioinspir Biomim* 2015; 10(3): 035005.

29. Onal CD and Rus D. Autonomous undulatory serpentine locomotion utilizing body dynamics of a fluidic soft robot. *Bioinspir Biomim* 2013; 8(2): 026003.

30. Meng C, Xu W, Li H, et al. A novel soft manipulator based on beehive structure. In: *IEEE/RSJ international conference on intelligent robots and systems (IROS)*, Hamburg, Germany, 28 September 2015–02 October 2015, pp. 2342–2347.

31. Marchese AD, Tedrake R, and Rus D. Dynamics and trajectory optimization for a soft spatial fluidic elastomer manipulator. *Int J Robot Res* 2015; 35(8): 1000–1019. DOI: 10.1177/0278364915587926.

32. Marchese AD and Rus D. Design, kinematics, and control of a soft spatial fluidic elastomer manipulator. *Int J Robot Res* 2015; 35(7): 840–869. DOI: 10.1177/0278364915587925.

33. Kramer RK, Majidi C, and Wood RJ. Wearable tactile keypad with stretchable artificial skin. In: *IEEE international confer-ence on robotics and automation (ICRA)*, Shanghai, China, 9–13 May 2011.

34. Kim YJ, Cheng S, Kim S, et al. A novel layer jamm-ing mechanism with tunable stiffness capability for

minimally invasive surgery. *IEEE Trans Robot* 2013; 29(4): 1031–1042.

35. Sun Y, Song YS, and Paik J. Characterization of silicone rubber based soft pneumatic actuators. In: *2013 IEEE/RSJ international conference on intelligent robots and systems*, Tokyo, Japan, 3–7 November 2013, pp. 4446–4453. IEEE.

36. Elsayed Y, Lekakou C, Geng T, et al. Design optimization of soft silicone pneumatic actuators using finite element analysis. In: *2014 IEEE/ASME international conference on advanced intelligent mechatronics*, Besancon, France, 8–11 July 2014, pp. 44–49. IEEE.

37. Nordin INAM, Razif MRM, Natarajan E, et al. 3-D finite-element analysis of fiber-reinforced soft bending actuator for finger flexion. In: *2013 IEEE/ASME international conference on advanced intelligent mechatronic*, Wollongong, Australia, 9–12 July 2013, pp. 128–133. IEEE.

38. Martinez RV, Glavan AC, Keplinger C, et al. Soft actuators and robots that are resistant to mechanical damage. *Adv Funct Mater* 2014; 24(20): 3003–3010.

39. Freyer H, Breitfeld A, Ulrich S, et al. 3D-printed elastomeric bellow Actuator for linear motion. In: *5th International conference on additive technologies*, Vienna, Austria, 15–17 October 2014.

40. Low JH. *Customizable soft pneumatic gripper devices*. Dissertation, 2015, http://scholarbank.nus.edu.sg/handle/10635/120577.

41. Onal CD, Chen X, Whitesides GM, et al. Soft mobile robots with on-board chemical pressure generation. In: *15th International Symposium on Robotics Research*, Flagstaff, Arizona, 28 August–1 September 2011, pp. 1–16. Springer.

42. Amend JR, Brown E, Rodenberg N, et al. A positive pressure universal gripper based on the jamming of granular material. *IEEE Trans Robot* 2012; 28(2): 341–350.